UC Davis
Geodynamica

Title
Mantle-Driven Environmental States during Supercontinent Assembly and Breakup

Permalink
https://escholarship.org/uc/item/2j625548

Journal
Geodynamica, 1(1)

ISSN
3065-2804

Authors
Coltice, Nicolas
ARNOULD, Maëlis
Husson, Laurent
et al.

Publication Date
2026-10-16

DOI
10.5070/F3.62175

Data Availability
The data associated with this publication are available at: https://osf.io/j8dav

Copyright Information
This work is made available under the terms of a Creative Commons Attribution License, available at https://creativecommons.org/licenses/by/4.0/

Peer reviewed

eScholarship.org Powered by the California Digital Library
University of California

Research Article

geodynamica

Mantle-Driven Environmental States during Supercontinent Assembly and Breakup

Nicolas Coltice [*1], **Maëlis Arnould** [2], **Laurent Husson** [3], **Jonathon Leonard** [4], **Marie Martin** [1], **Loïc Pellissier** [5,6], **Julian Rogger** [7], **Tristan Salles** [4], **Sabin Zahirovic** [4]

[1] *Université Côte d'Azur, CNRS, OCA, IRD, GEOAZUR, France*
[2] *Université Lyon 1, ENS de Lyon, UJM, CNRS UMR 5276, LGL-TPE, Villeurbanne, France*
[3] *CNRS, ISTerre, Université Grenoble-Alpes, Grenoble, France*
[4] *School of Geosciences, The University of Sydney, Sydney, Australia*
[5] *Department of Environmental Systems Science, ETH Zurich, Zurich, Switzerland*
[6] *Unit of Land Change Science, Swiss Federal Research Institute WSL, Birmensdorf, Switzerland*
[7] *School of Geographical Sciences, University of Bristol, Bristol, United Kingdom*

Abstract

How the formation and breakup of supercontinents drive environmental shifts remains a fundamental question, but piecemeal deep-time records prevent an answer based on observations. Here we present the first simulation of an Earth-like planet integrating geodynamics, climate, and surface processes to assess how solid Earth dynamics regulate environmental change. We show that mantle flow governs surface conditions through two coupled pathways: true polar wander (TPW) and seafloor spreading rate. During supercontinent assembly, a large-scale mantle flow draws continents together and, through TPW, aggregates the landmasses toward the equator, while seafloor production decreases and the seafloor ages. The larger tropical land area increases planetary albedo and continental weatherability, while reduced seafloor spreading lowers mantle degassing; together these effects suggest a cooling of the atmosphere while the mantle warms. During breakup, the switch to smaller-scale mantle flow reverses both pathways: continents drift as seafloor rejuvenates, lowering tropical albedo and weatherability while increasing degassing and sea level, which together warm the atmosphere as the mantle cools. These internally generated, mantle-driven shifts reproduce key features of Pangea on Earth, providing a mechanistic framework linking deep Earth dynamics to climate and, ultimately, to conditions for life.

Editor(s):
Stephane Mazzotti
Meng Guo
Thibault Duretz
Production:
Mohamed Gouiza

Reviewers:
Douwe van Hinsbergen
Anonymous reviewer

Submitted:
23 January 2026
Accepted:
21 September 2026
Published:
16 October 2026

1 Introduction

Throughout geological history, continental blocks aggregate and form vast landmasses, called supercontinents, that ultimately fragment and drift over hundreds of millions of years (*Pesonen et al.*, 2021). The progressive amalgamations of continents and their breakups have provided an instrumental perspective for interpreting the geological record, linking deep lithospheric changes to environmental changes (*Veevers*, 1990; *Bradley*, 2011; *Nance et al.*, 2014).

Being the most recent supercontinental event, Pangea is the most detailed case study owing to the better preservation of the geological archive. It assembled approximately 325 million years ago, uniting Gondwana and Laurasia near the equator, before initiating a breakup by rifting and seafloor spreading some 200 million years ago. Pangea aggregation progressively built up the Alleghanian-Variscan orogenic belt, comparable in scale to the modern Himalayas, stretching across present-day Africa, the Americas, and Eurasia (*Maierová et al.*, 2016). This mountain building has been proposed to be concomitant with a substantial global cooling lasting about 70 Myr, called the Late Paleozoic Ice Age (*Montañez and Poulsen*, 2013), as evidenced by the expansion of ice sheets to lower latitudes and sea level fall by several hundred meters (*Veevers*, 1990; *Guillaume et al.*, 2016). After supercontinent assembly, Earth's climate likely underwent a warming phase, which culminated in a greenhouse climate state during the Cretaceous coinciding with supercontinent dispersal and the emplacement of large igneous provinces (*Sun et al.*, 2012; *Scotese et al.*, 2021; *Rogger et al.*, 2024). Sedimentary archives record a transition from widespread glacial deposits and unconformities, i.e., low sea level, during assembly to the formation of extensive continental basins during breakup (*Golonka and Ford*, 2000). Similar coupled tectonic-climatic patterns are inferred for earlier supercontinents, including Rodinia, Columbia, and Kenorland, underscoring the fundamental role of supercontinents as a first-order regulator of Earth's long-term climate (*Nance*, 2022). Carbon-climate modelling studies suggest that the aggregation of Pangea disrupted oceanic circulation patterns and contributed to the aridification of continental interiors (*Crowley*, 1994; *Scotese et al.*, 2021). Meanwhile, enhanced chemical weathering of newly formed mountains facilitated the drawdown of atmospheric CO_2 (*Goddéris et al.*, 2017). However, generalities can hardly be drawn, and the question of how supercontinent formation and breakup shape the surface environment remains open.

*✉ nicolas.coltice@oca.eu

The aggregation of multiple continents into large supercontinents is both an expression and a driver of Earth's mantle convection. For continents to collide, mantle flow requires large-scale subduction zones to draw the landmasses together (*Gurnis*, 1988). *Zhong et al.* (2007) proposed that the corresponding mantle flow is dominated by spherical harmonic degree 1, which corresponds to a hemispheric downwelling and upwelling structure. When the supercontinent is formed, depending on its size, the temperature below can warm by several tens of degrees (*Coltice et al.*, 2007; *Rolf et al.*, 2012). To break up and disperse the continental masses, the subduction configuration has to profoundly change. *Zhong et al.* (2007) suggested that spherical harmonic degree 2 of the flow dominates, which corresponds to a structure close to that of Earth's present-day mantle (*Ricard and Bai*, 1991). Convection models self-generating plate-like behaviour and continental drift have corroborated these ideas (*Rolf et al.*, 2012), and have shown that the stress ratio between the strength of the lithosphere and viscous stresses emerging from mantle flow plays a dominant role: a strong lithosphere generates the large-scale mantle flow required for continental aggregation but if too strong, continents never break up (*Rolf et al.*, 2014). Once they form, supercontinents can warm the underlying mantle by two processes: insulation of the mantle beneath and the generation of a larger-scale flow that is less efficient for mantle heat transfer (*Coltice et al.*, 2007; *Phillips and Coltice*, 2010; *Lenardic et al.*, 2011; *Rolf et al.*, 2012). The process of supercontinent formation is therefore a phenomenon defining a very specific thermal and flow structure of mantle convection.

A central scientific challenge, therefore, is to determine if and how these profound changes in mantle dynamics that occur during the formation and breakup of a supercontinent lead to predictable first-order environmental changes. Although conceptual links exist – such as the proposed control of the style of mantle flow below supercontinents on the atmosphere (*Jellinek et al.*, 2020) – a unified physical framework linking deep-mantle dynamics to surface environmental change remains elusive. The connections between seafloor spreading and sea level (*Conrad*, 2013; *Young et al.*, 2022), and paleogeography and climate (*Mills et al.*, 2017; *Bufe et al.*, 2024) thus remain disconnected from each other. This integration is precluded by fundamental uncertainties in deep-time constraints, particularly on paleo-topography (*Scotese*, 2021) and mantle degassing fluxes before 100 Ma (*Seton et al.*, 2023), as well as by modelling unknowns and uncertain mantle properties.

To overcome the reconstruction limitations, we developed a fully integrated simulation of an Earth-like planet, building on a mantle convection model that self-consistently produces plate-like tectonics over billion-year timescales (*Coltice et al.*, 2019). The resulting synthetic planet, hereafter referred to as *Pandora*, reproduces deep Earth dynamics and its surface expressions (*Arnould et al.*, 2020; *Frasson et al.*, 2024; *Janin et al.*, 2025), providing a continuous physical record unavailable on Earth. Using climate and surface process models calibrated on Earth data (i.e., not tuned to make Pandora fit Earth observations), we focus on its supercontinent phase (Figure 1) and assess how mantle flow changes translate into environmental evolutions (climate and landscape). Our models show that supercontinent aggregation involves a mantle state that generates a specific TPW signature, as well as a slowdown of seafloor production rate. The breakup phase initiates with a rejuvenation of the seafloor before the supercontinent actually splits into pieces. These effects profoundly shape the state of the external envelopes in the models, helping to interpret the transition observed between icehouse and hothouse states of Pangea.

2 Integrated Modelling from Mantle to Surface

2.1 From Mantle Convection to Planetary Geography

Understanding how mantle flow shapes climate and surface processes requires an integrated framework, because tectonics, surface evolution, and climate drive chemical and energy fluxes across timescales (*Lenardic et al.*, 2016). Here we combine global 3D climate and landscape models with the only 3D spherical mantle convection calculation published to date that self-consistently generates the major tectonic features of Earth at Earth-like convective vigor (*Coltice et al.*, 2019), i.e., producing Earth-like global heat flow, surface velocities and elevation distribution (*Arnould et al.*, 2018), one-sided subduction, transforms, plate reorganizations (*Janin et al.*, 2025), rifting and collision, plume dynamics (*Arnould et al.*, 2020) and TPW (*Frasson et al.*, 2024) over 1 Gyr of evolution. This numerical solution, called Pandora, corroborated the overall dominance of the role of subduction in plate kinematics, as already proposed (*Forsyth and Uyeda*, 1975; *Conrad and Lithgow-Bertelloni*, 2002). But this dominance fluctuates: it is the strongest when rifting and breakup of continents arise, whereas dragging from the mantle reaches its maximum (driving about 40% of the total area of tectonic plates) when the continents are in the process of aggregating (*Coltice et al.*, 2019).

Pandora is a 3D spherical numerical solution of mantle convection produced with the code StagYY (*Tackley*, 2008) using the Boussinesq approximation at high resolution in space (23 km on average vertically and laterally with higher vertical resolution near the top and bottom) and in time (typical time step of 3000 years). The model parameterization and numerical solution are detailed in *Coltice et al.* (2019).

Continents are imposed through thick (200 km), buoyant and resistant lithospheric rafts, surrounded by more deformable, more buoyant and thinner (125 km) belts. Their initial shape and position correspond to Earth's continent location at 200 Ma. Continental drift together with plate-like tectonics arises self-consistently from mantle convection thanks to the use of a pseudo-plastic rheology. In such a model, neither plate geometry nor kinematics is imposed. Once the model starts, continents move according to the balance between viscous stresses, pressure gradients and buoyancy. Although these continents are highly simplified and do not account for a light continental crust, the choice of continental lithosphere density ensures that the hypsometry of the models is bimodal. The Rayleigh number of Pandora (10^7) was chosen to generate a convective vigour similar to Earth, as characterized by the measurable surface

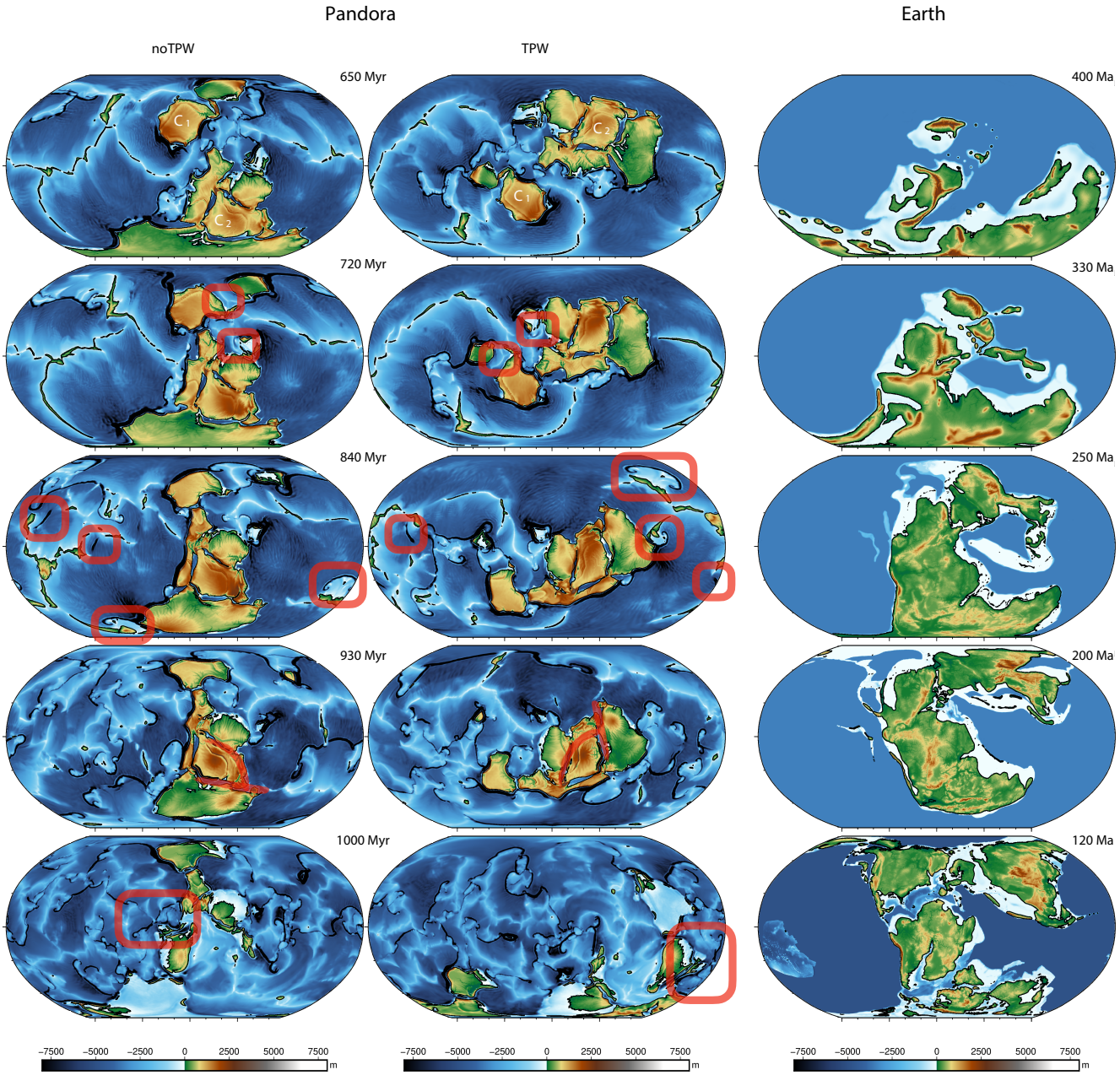


FIGURE 1 – Paleogeographic evolution of Pandora and Earth over supercontinent assembly and breakup. Left column: Pandora with 1 Earth ocean volume without accounting for TPW. Central column: Pandora with 1 Earth ocean volume accounting for TPW. Right column: Earth during Pangea times (*Scotese*, 2021). C_1 and C_2 denote the two large landmasses that ultimately assemble. Red boxes and lines highlight the tectonic features discussed in the text (rifts and trenches).

expressions described above.

Although Pandora is a unique and advanced simulation, it relies on assumptions that make the calculation tractable, in a context where solving convective flow with the full physics and known parameters of terrestrial rocks remains beyond current computational capabilities. Among these assumptions, the rheology of rocks at low temperature is simplified, particularly for continental lithosphere. Consequently, some of the tectonic structures produced by Pandora are not fully realistic: slab edges do not tear sharply but instead tend to curl inward; mountains form but display a plateau-like morphology with steep margins rather than the high-relief signature expected from rapid exhumation; and elongated transform structures develop but rarely persist over more than tens of millions of years. Mantle flow in Pandora is also treated as incompressible and neglects melting and phase transformations. Nonetheless, as noted above, it remains the most advanced simulation to date that self-generates surface tectonics, producing synthetic observations close to what is expected for Earth.

To translate geodynamics into planetary geography, we compute elevations and adopt the Tisserand reference frame, where the degree-2 geoid defines the principal axis of inertia and thus TPW (*Goldreich and Toomre*, 1969). In addition, we also consider the reference frame corresponding to no net rotation of the surface, the comparison between the two enabling us to disentangle plate motions and TPW, something impossible for Earth reconstructions (*Leonard et al.*, 2025).

Due to the use of free-slip boundary conditions, surface topography (h) is calculated from stresses normal to the surface (σ_{rr}) below the surface following:

$$h = \frac{\sigma_{rr}}{\Delta\rho g} \quad (1)$$

where $\Delta\rho$ corresponds to the model internal density variations and g is the gravitational acceleration. The resulting topography field accounts for both lateral and radial static density differences within the lithosphere (isostatic topography) and those resulting from mantle convection (dynamic topography).

In order to estimate the topography-bathymetry distribution, we first need to correct the surface topography field to account for the effect of ocean loading. To do so, we incrementally add a given volume of water in order to progressively flood the topography while correcting it to account for water density. We ran two cases: one with an initial volume corresponding to 1 Earth ocean (1.34×10^9 km^3) and the other corresponding to 1.5 Earth ocean volumes (Figure S1). We compute sea level changes through the evolution of the distance between the water surface and the planetary center of mass.

In the model, the continental budget is set at the onset of the simulation and can only decrease by progressive recycling in the mantle. Modelling continent production is beyond the capabilities of our model. We therefore compensate for the impact of the progressive loss of continents on sea level by increasing the volume of oceans through time at a rate of $e \times \bar{d}$, where $e = 0.15$ km^2 y^{-1} is the average continental area loss through time (*Coltice et al.*, 2019) consistent with present-day estimates of both erosional and accretionary margins (*Clift and Vannucchi*, 2004), and $\bar{d} = 3.8$ km is the average ocean depth on Earth.

2.2 From Planetary Geography to Climate

Climate dynamics are simulated using the intermediate-complexity coupled ocean–atmosphere general circulation model PLASIM-GENIE (*Holden et al.*, 2016). The parameterization is described in *Holden et al.* (2016) and *Leonard et al.* (2025) and is set for Earth, not specifically for Pandora. We hence test how a climate system operating as on Earth responds to the orientation towards the star and the distribution of elevation relative to sea level provided by Pandora.

The model operates at a horizontal resolution of 5.6°×5.6° (∼600 km along a meridian), with 10 vertical atmospheric layers and 16 oceanic layers. To preserve land bridges and ocean gateways at this coarse resolution, land–ocean connectivity is maintained using a skeletonisation algorithm (*Leonard et al.*, 2025). PLASIM-GENIE couples the atmosphere (PUMA) and vegetation (ENTS) modules from PLASIM with the ocean (GOLDSTEIN) and sea-ice (GOLDSTEINSEAICE) modules from GENIE (Figure 1 in *Holden et al.*, 2016). The PUMA three-dimensional spectral atmospheric model is described in *Fraedrich et al.* (1998, 2005), the ENTS surface and vegetation model in *Williamson et al.* (2006), and the three-dimensional frictional-geostrophic ocean and zero-dimensional dynamic-thermodynamic sea-ice models in *Edwards and Marsh* (2005). The current configuration has been extensively benchmarked against present-day climate observations (*Holden et al.*, 2019).

PLASIM-GENIE has previously been used to simulate deep-time climate ensembles spanning more than 100 Myr (*Leonard et al.*, 2025), yielding an average equilibrium climate sensitivity of 3.6 °C. The same workflows are employed here, including skeletonisation to preserve paleogeographic connectivity at low resolution and an atmosphere–ocean gearing strategy in which atmospheric fluxes are updated once every 10 years. This configuration enables efficient simulations, requiring approximately 24 hours on a single CPU to reach 2000 model years.

Except for geography, all boundary conditions are held constant, with the solar constant set to its present-day Earth value. Atmospheric CO_2 is fixed at 1035 ppm to both approximate the Phanerozoic mean (*Goddéris and Donnadieu*, 2019) and simplify the climate modelling since such a concentration generates ice-free solutions. Each simulation is spun up to quasi-equilibrium over 2000 model years. Full details of the workflow used to apply PLASIM-GENIE across large deep-time ensembles are provided in *Leonard et al.* (2025). These simulations yield evolving global fields of temperature and precipitation across the geodynamic cycle.

In principle, full coupling with a dynamic carbon cycle would be preferable. However, computational constraints restrict this study to a single CO_2 scenario representative of Earth's long-term mean climate state. This approach provides precipitation patterns suitable for landscape evolution modelling, while long-term climate variability is inferred a posteriori from the geodynamic and surface data rather than explicitly simulated. Because CO_2 is fixed here, the simulated climate states respond to paleogeography only, which shifts at tectonic rates. Hence, we compute climate states at 10 Myr intervals.

2.3 Surface Processes

Finally, we combine geodynamics and climate with goSPL (*Salles et al.*, 2020, 2023a), a scalable, open-source numerical framework designed for parallel computation of landscape and sedimentary basin evolution at the global scale, here at a spatial resolution of ∼5 km. The model incorporates the main long-term drivers of topographic change, namely river incision and hillslope diffusion, and explicitly tracks sediments from their sources to depositional sinks. This includes alluvial and marine deposition, compaction, porosity evolution, and the reconstruction of stratigraphic architectures. The system can be forced with both spatially and temporally varying tectonic boundary conditions (vertical and horizontal displacements) as well as climatic histories, such as precipitation variability and sea level change. The parameterization of goSPL used in the simulations for Pandora is that calibrated for Earth (*Salles et al.*, 2023a). Thus, we explore how Earth-like surface processes would respond in the context of Pandora.

The governing equation is based on mass conservation and takes the general form:

$$\frac{\partial z}{\partial t} = U + \kappa\nabla^2 z + \epsilon P^d (PA)^m |\nabla z|^n \quad (2)$$

where z is the surface elevation, t is time, and U represents tectonic forcing (uplift rate, in $m\ yr^{-1}$). The second term describes hillslope diffusion, with κ set to 0.5 $m^2\ yr^{-1}$ (*Salles et al.*, 2018). Fluvial incision follows the stream power law, with $m = 0.5$, $n = 1$, and erodibility ϵ fixed at $8.0e^{-7}\ yr^{-1}$. Water flux (PA) results from the upstream contributing area (A) weighted by climate precipitation and evapotranspiration (P) (*Salles et al.*, 2018). To capture the influence of precipitation on weathering and incision, ϵ is further scaled by mean annual rainfall using an exponent $d = 0.42$, consistent with field-based studies (*Murphy et al.*, 2016). In this formulation, deposition is zero along flat or gently inclined surfaces, but accumulation occurs in depressions and closed basins. Sediment transport is linked to erosion in headwater catchments through a multiple-flow routing algorithm that distributes both runoff and sediment flux across several downstream pathways. This avoids artificial channel locking and improves flux partitioning at the basin scale. At the global level, water discharge (PA) is calculated using the parallel implicit drainage area (IDA) approach (*Richardson et al.*, 2014; *Salles*, 2019), implemented on a spherical mesh as a sparse matrix system with diagonal unity terms and off-diagonal neighbour connections. The IDA problem is solved with the Richardson iterative method and block Jacobian preconditioning (*Richardson et al.*, 2014), both integrated into PETSc (*Balay et al.*, 2012). Sediment transport uses an analogous formulation (*Salles*, 2019). A key strength of goSPL is its implicit and parallel solver design (*Salles*, 2019), which (1) ensures numerical stability even with large time steps, and (2) enables efficient scaling across hundreds of processors.

Landscapes in goSPL are reconstructed using time-dependent elevation maps from Pandora together with associated climatic boundary conditions. Both elevation and precipitation maps are resampled onto an icosahedral mesh with >10 million nodes (~5 km global resolution). Tectonic forcing is imposed by differencing successive freeboard elevations and accounting for horizontal surface advection extracted from the mantle convection velocity field. For each 1 Myr time slice, a simulation was performed on 168 CPUs, with outputs archived as NetCDF grids.

3 Mantle-to-Surface Evolution During Supercontinental Assembly and Breakup

After an initial spin-up phase of rapid plate reorganizations, Pandora produces a supercontinent that quickly fragments at around 300 Myr before gradually assembling into two major continental domains (see Movie S1). These ultimately aggregate into a long-lived supercontinent at ~720 Myr, driven by large-scale mantle flow associated with the formation of a subduction zone of hemispheric scale (*Janin et al.*, 2025). The fully assembled supercontinent remains stable for ~200 Myr (Figure 1). New subduction zones initiate in the oceans and along continental margins, accompanied by more mantle plumes coming from the base of the model reaching the surface at ~850 Myr. Breakup begins with the propagation of rifting from the ocean into the continent to split a small fragment, while the main landmass remains intact until ~930 Myr. At this time, final breakup occurs along two rift branches connected at a triple junction. One branch aborts, the other evolves into a spreading ridge. Renewed rifting 15 Myr later divides the supercontinent into three major blocks by 1000 Myr (Figure 1). This phase features rapid seafloor rejuvenation and extensive continental stretching, with sea level increasing by ~100 m and causing major continental flooding.

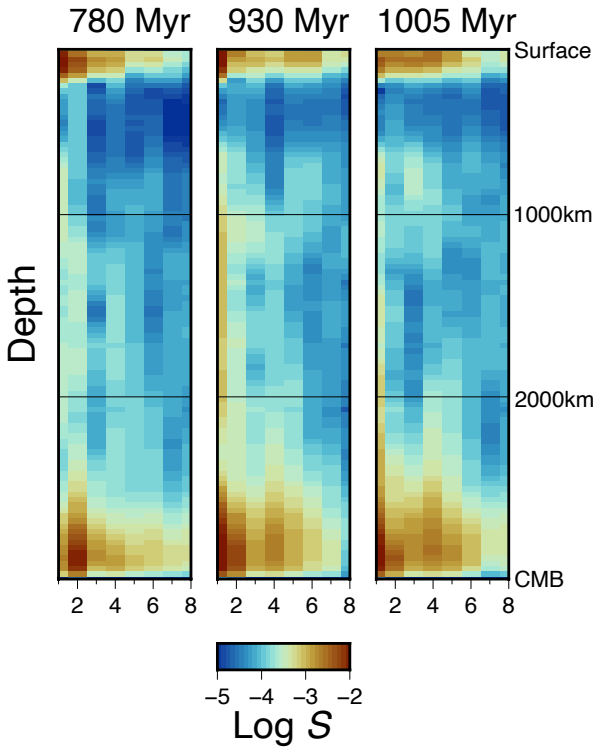


FIGURE 2 – Evolution of the normalized spectral power S of the temperature field heterogeneity as a function of depth and spherical harmonic degree in Pandora. When the supercontinent is formed at 720 Myr, the longest wavelengths are dominant close to the surface. With the progressive rejuvenation of the seafloor and breakup, larger degrees gain spectral power over degree 1 (930 and 1005 Myr).

During the assembly phase, the thermal structure of the upper mantle is dominated by very long-wavelengths and a strong spherical harmonic degree 1 (Figure 2) in agreement with *Zhong et al.* (2007), which corresponds to the large-scale subduction zone attracting the continental blocks (Figure 3). During this phase, the seafloor production rate is stable and at its lowest (Figure 4), with ocean floor progressively aging. This type of configuration is typical for low heat flow and surface velocity as very long-wavelengths are not optimal for heat transfer (*Grigné et al.*, 2005; *Phillips and Coltice*, 2010). Hence the mean mantle temperature increases by about 10 K over 100 Myr and reaches its maximum by 850 Myr (Figure 4). The rise in mantle temperature destabilizes the lithosphere, as the density difference between the two increases and the viscosity of the mantle decreases. As a consequence, new subduction initiates, rejuvenating the seafloor and cooling the mantle (Figures 1 and 4). The thermal structure of the upper mantle becomes dominated by smaller wavelengths (spherical harmonic degrees 2 to 6, see Figures 2 and 3), consistent with previous modelling (*Rolf et al.*, 2012).

The evolution of thermal structure of the mantle has

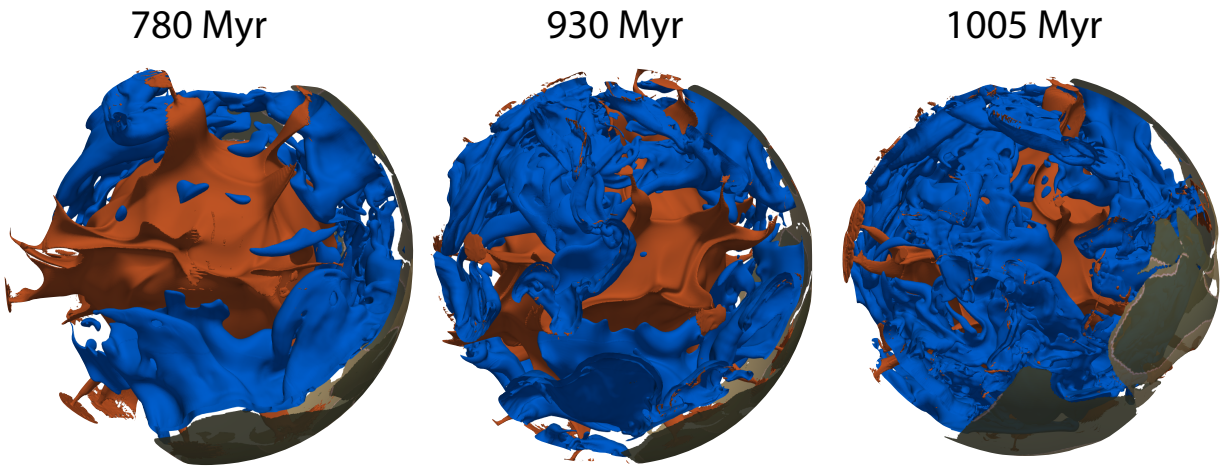


FIGURE 3 – Evolution of the 3D thermal structure in Pandora. Continents at the surface are in olive green: dark olive green represents the strong nucleus and lighter olive green represents the more deformable belts. Isotherm 1350 K represents edges of downwellings. Isotherm 1845 K represents edges of plumes. The snapshots on this figure correspond to the thermal heterogeneity spectra in Figure 2.

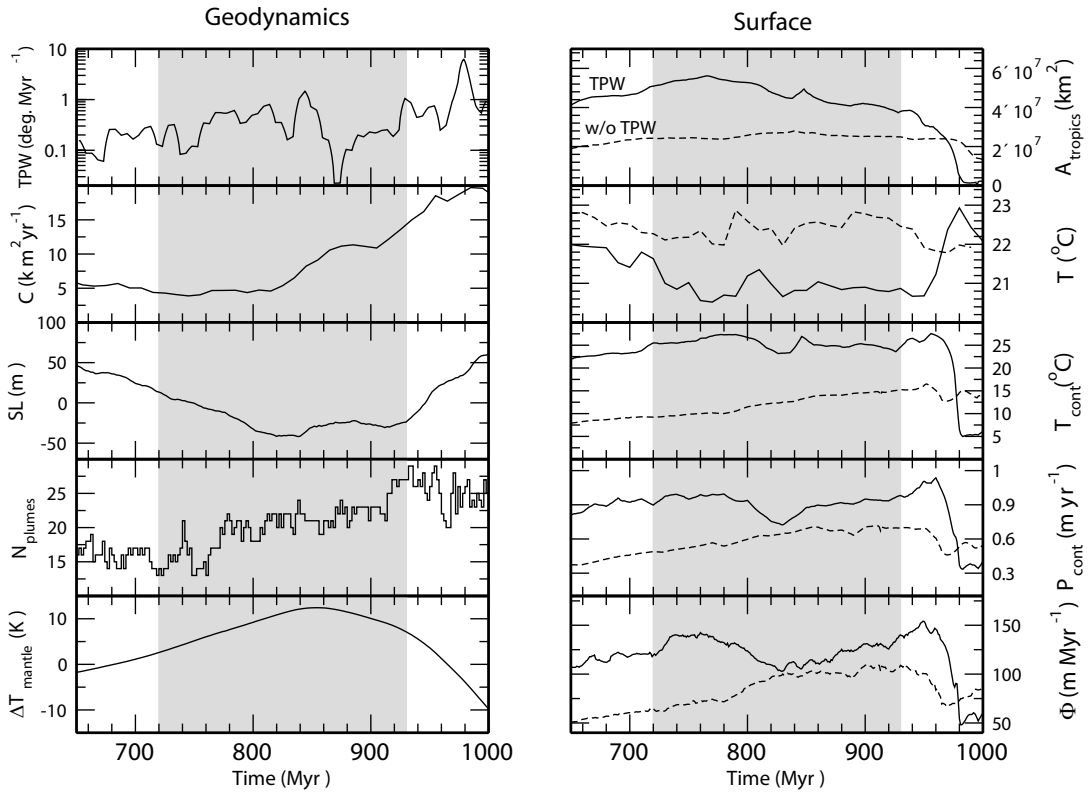


FIGURE 4 – Time series of Pandora evolution through supercontinent assembly and breakup. Left: Time series of geodynamic features being true polar wander velocity (TPW), seafloor production rates (C), sea level change (SL), number of plumes (N_{plumes}) and temperature change of the mantle (ΔT_{mantle}) for Pandora. Right: Time series of surface features being continental area in the tropics (A_{tropics}), mean surface temperature (T), mean continental surface temperature (T_{cont}), precipitation rate (P_{cont}), and flux of material eroded (Φ) (with and without accounting for TPW). The background colour shift from white to grey marks the onset of the supercontinent, and the following shift from grey to white the first breakup.

strong consequences for TPW. During the assembly phase, TPW proceeds at a steady, slow rate of $\sim$0.3° Myr^{-1} (Figures 4 and S2). This solid-body reorientation preferentially brings the hemispheric trench system close to the equator, ultimately producing collision within the tropics (Figure 1), an effect specific to TPW. The model without TPW does not reproduce this behaviour (Figure 1).

To test this, we built a null distribution by randomly drawing 300 alternative reference frames (i.e., alternative orientations of the spin axis relative to the mantle flow field; see Figure S3 for the sampled poles) and, for each, computing the fraction of seafloor subduction occurring at low latitudes (between $-40°$ and $40°$). We then compared this null distribution to the equivalent value obtained in the Tisserand reference frame, in which the geographic pole coincides with the true spin axis (as required to account for TPW). The TPW-consistent configuration ranks in the upper quartile of the null distribution, indicating that TPW systematically drives large-scale subduction toward low

latitudes during the aggregation phase (Figure 5). This result is consistent with sensitivity tests on more idealized systems featuring a single elongated subduction zone and a viscosity increase in the lower mantle (*Ricard et al.*, 1993; *Greff-Lefftz and Besse*, 2014).

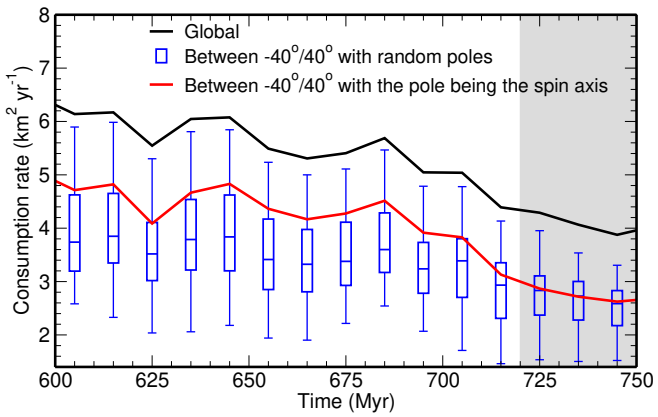


FIGURE 5 – Statistical significance of low-latitude trench concentration driven by TPW. Blue boxplots show the null distribution of low-latitude ($-40°$ to $40°$) seafloor consumption rate at each time step, obtained by randomly rotating the modeled geography to 300 alternative poles (Figure S3) and recomputing the consumption rate for each. Red line shows the actual low-latitude consumption rate in the Tisserand reference frame, which accounts for TPW. The total consumption rate of the model is represented in black.

When collision is complete and the detached slabs begin sinking into the lower mantle around 750 Myr, TPW reverses direction (Figure S2) and progressively accelerates to 0.5–1° Myr^{-1} (Figure 4), again consistent with these sensitivity tests (*Ricard et al.*, 1993; *Greff-Lefftz and Besse*, 2014). TPW briefly spikes to 1° Myr^{-1} at 840 Myr as new slabs sink into the upper mantle, before slowing and stabilizing (Figures 4 and S2). It then accelerates sharply, peaking near 6° Myr^{-1} roughly 50 Myr after breakup (Figure 4), as the merging of trenches rapidly tears a continental block apart.

The convective evolution of the mantle also shapes the elevation distribution of the model, and hence sea level. During the aggregation phase, seafloor progressively ages and ocean basins deepen (Figure 1). Therefore, sea level falls at a rate of $\sim$0.5 m Myr^{-1} (Figure 4). When the supercontinent is formed, sea level continues to drop, reaching a minimum around 830 Myr (Figure 4). The seafloor then rejuvenates with larger production rates, hence sea level rises by about 20 m and stays constant until breakup initiates, where it rises at $\sim$1 m Myr^{-1} (Figure 4).

Mantle convection, through TPW and seafloor spreading, leads to strong surface consequences. In the model with TPW, the average surface temperature computed with the climate models cools by 1.5 °C, whereas in the simulation without TPW the temperature remains constant (Figure 4). Because all other climate parameters are held fixed and the climate evolves gradually, this cooling results solely from the rotation of the geography. The key difference between the two geographies is the continental area located in the tropics (rows 1-4 in Figures 1 and 4), which determines tropical albedo. As the tropics receive the most intense incoming solar radiation, a larger continental area there reflects more radiation back to space, moderately cooling the climate. After breakup, continents drift poleward, tropical albedo declines and global temperature rises by $>2°$C, returning to pre-assembly values.

Also, low latitude aggregation promoted by TPW impacts the hydrological cycle and hence the landscapes: it first intensifies erosion and eroded material fluxes to the oceans when elevated areas enter wet tropical belts (Figures 4 and 6), whereas later transient plume-driven uplift on the far-eastern continental margin (800–840 Myr), situated in the tropics, blocks moisture transport into the interior and temporarily reduces erosion (Figure 6). At 780 Myr (Figure 4), the eroded material flux peaks, corresponding to a maximum of both emerged land and elevation in tropical area. Both the 1$\times$ and 1.5$\times$ ocean volume scenarios yield similar trends (Figure S7). Through breakup, landmasses are progressively flooded and escape tropical area. At first, precipitation intensifies but eventually shift to smaller, low-relief landmasses, causing erosion rates to collapse by 50% within 40 Myr after the start of the dispersal (Figures 4 and 6).

4 Discussion

4.1 Predicted Environmental States Over the Supercontinent Assembly and Breakup

The results of our modelling suggest that the mantle evolves through two states during a supercontinent cycle:

- an aggregating state that starts more than 100 Myr before the supercontinent is formed. This state is characterized by a very large-scale flow featuring a hemispherical trench structure. Such large-scale flows produce TPW, which brings this structure within low latitudes. It also corresponds to less efficient heat loss from the mantle, being characterized at the surface by aging of the seafloor and a slight warming of the mantle.
- a breakup state that initiates 50–100 Myr before the effective continental separation. The scales of mantle flow are smaller, with subduction initiations and new mantle plumes. Heat transfer becomes more efficient and the mantle cools. The surface expression is a rejuvenation of the seafloor with an increase in seafloor production rate. The initiation of new subduction zones and the sinking of the slabs that drove aggregation into the lower mantle change the TPW path, with potential peaks in velocity.

From the climate and surface processes modelling, we suggest that these two states shape a shift in the surficial environment. Firstly, the geography of the aggregation state is dominated by the collision of the continental pieces happening preferentially at low latitudes because of TPW. Combined with the low sea level and hence the larger amount of exposed land, it increases the albedo and contributes to cooling the global climate.

Secondly, we expect the aggregation state to strongly impact atmospheric pCO_2 and hence climate. We do not model here how pCO_2 and climate would co-evolve self-consistently in Pandora; however, we can qualitatively

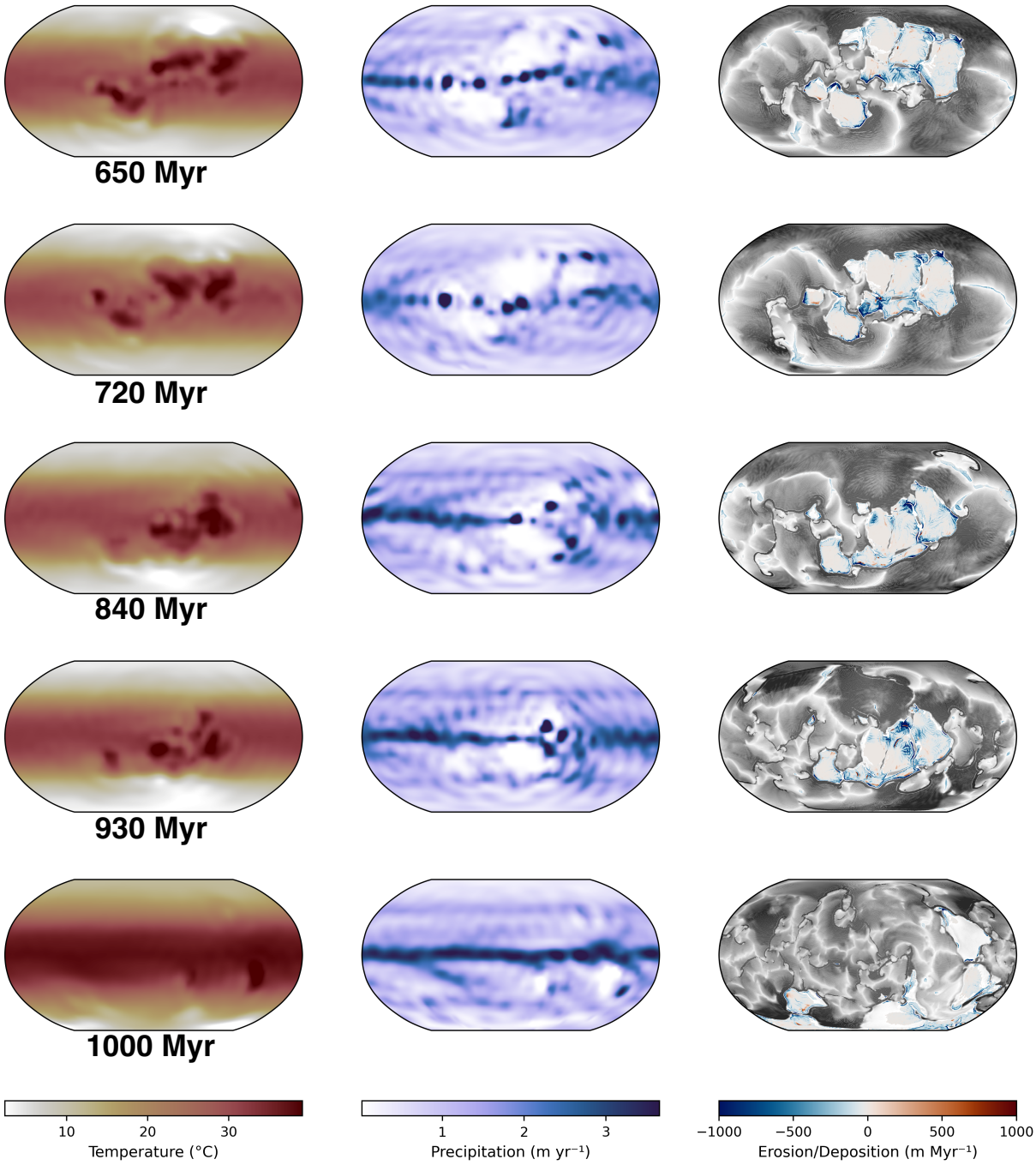


FIGURE 6 – Climate and surface processes evolution of Pandora over supercontinent assembly and breakup. The model is with 1 Earth ocean volume and accounts for TPW. Left column: Temperature. Central column: Precipitation. Right column: Erosion and deposition.

assess how they should evolve during the aggregation state. Atmospheric pCO_2 varies on million-year timescales as silicate weathering balances mantle degassing (*Arnscheidt and Rothman*, 2022), co-evolving with surface temperature and precipitation (*Walker et al.*, 1981). Assuming that degassing at ridges, subduction zones, and plumes scales with seafloor production rate (*van Der Meer et al.*, 2014) and carbon concentrations in mantle sources do not vary significantly over 350 Myr, degassing is then minimal during aggregation. Because weathering balances degassing at geological timescales, the two fluxes are ultimately equal and follow the same trend. The CO_2 weathering flux depends on local temperature, precipitation, and erosion rates (*West*, 2012), such that the atmospheric pCO_2 required to sustain a given flux depends on landscape "weatherability". More weatherable landscapes achieve higher weathering fluxes at lower pCO_2 and cooler climates than less weatherable ones. In the aggregation state, continental temperature, precipitation, and erosion are all maximized, owing to TPW bringing the collision zone into the tropics and to low sea level (Figure 4). Weatherability tends therefore to be optimal, suggesting that the planet can match the degassing flux with weathering at relatively low pCO_2 and low temperature.

The breakup state is the opposite. The rejuvenation of the seafloor and the arrival of new plumes increase the degassing flux. TPW could coincidentally keep the continents within low latitudes, depending on where subduction

initiates and propagates. Sea level rises and less land is exposed. Weatherability is therefore expected to decrease, suggesting that matching a larger degassing flux requires higher pCO_2 and temperature than in the aggregation state.

Taken together, these results suggest that global climate cools prior to effective supercontinent assembly, and then warms before and during breakup, as seafloor rejuvenation and plume activity increase degassing and drive sea level rise.

4.2 Pandora vs. Earth Reconstructions

Reconstructing Earth's evolution is intrinsically limited by the incompleteness of the geological archive. The absence of an oceanic crust record older than ∼200 Ma is limiting, which leads to the use of indirect observations to reconstruct global seafloor production and degassing (*van der Meer et al.*, 2017; *Müller et al.*, 2022). The difficulty of accurately defining reference frames hinders the separation of TPW from plate motions (*Tetley et al.*, 2019; *Wagenaar et al.*, 2025). Continental paleoelevations and uplift rates are likewise uncertain as reconstructions go deeper in age (*Scotese*, 2021).

Pandora provides a continuous, self-consistent framework that directly addresses these limitations by generating co-evolving mantle flow, plate motions, topography, climate, and erosion fields. Expanding the modelling proposed here would also allow testing the sensitivity of the planetary system to variations in its physical parameters. The main difficulty, however, is computing time, as realizing one experiment takes at least 6 months to generate the geodynamic model, and several additional months to complete the full workflow with climate and surface process models. Despite simplified rheological and continental models, Pandora reproduces the first-order surface evolution attributed to Pangea and Rodinia, although sometimes with larger amplitudes: sea level fall and expanded emerged area during assembly, peak elevations during the stable supercontinent stage, and renewed flooding before breakup (Figures 1, 4 and 7; *van der Meer et al.*, 2017; *Marcilly et al.*, 2022; *Young et al.*, 2022). Crucially, Pandora identifies the underlying drivers: the large-scale mantle flow leading to supercontinental assembly and its switch to smaller-scale flow impact both paleogeography — through TPW — and seafloor spreading.

Supercontinent amalgamation at low latitudes is a recurring pattern in Earth history. Gondwana was in a south polar position before drifting northward to collide with Laurasia at low latitude, forming equatorial orogens (*Blakey*, 2008); Rodinia's assembly also happened at low latitudes (*Evans*, 2021). TPW, which represents the long-wavelength geoid evolution, is an integrated signal as it reflects the whole density distribution within the Earth. Geodynamic studies show that subducting plates dominate the signal of the long-wavelength geoid (*Greff-Lefftz and Besse*, 2014). In Pandora, aggregation is driven by a hemispheric subduction zone that creates a positive degree-2 geoid, pulling the trench toward the equator until compensated by the presence of deep slabs at ∼1500 km depth. This mechanism explains the observed equatorial drift. The topology of the large-scale trench system and the distribution of deep

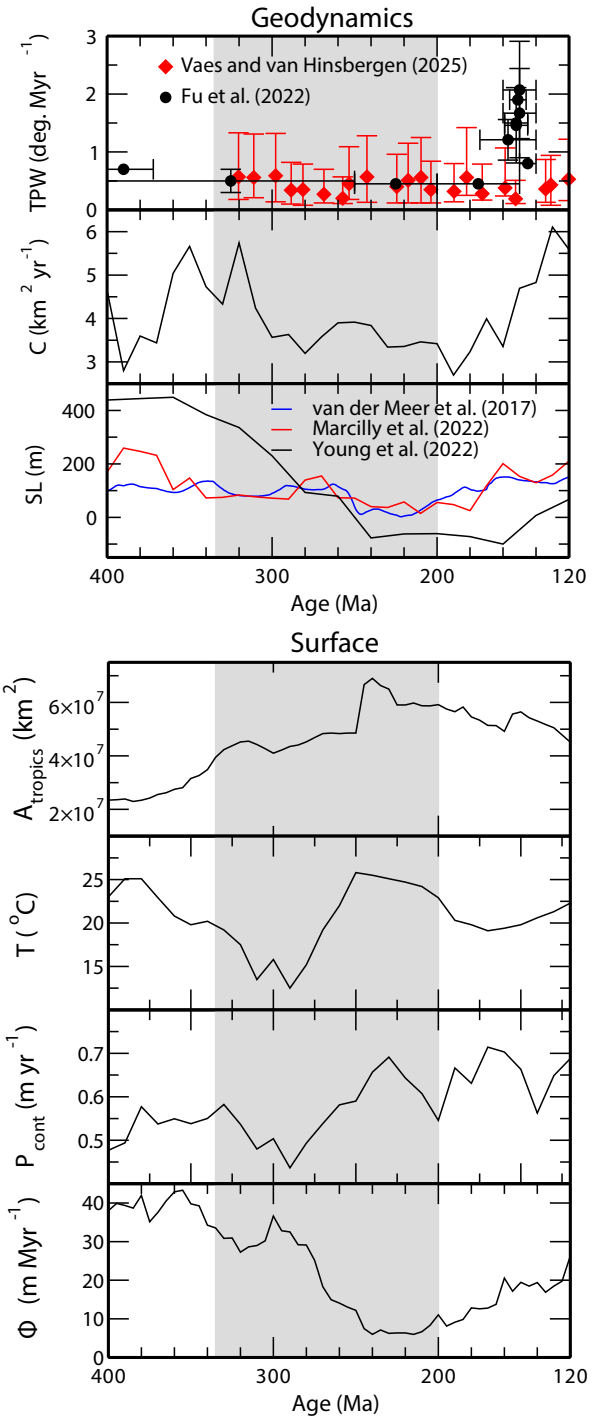


FIGURE 7 – Time series of Earth system evolution through Pangea assembly and breakup. Top: Time series of geodynamic features on Earth being TPW velocity (data: black circles from *Fu et al.* (2022) and red diamonds from *Vaes and van Hinsbergen* (2025)); seafloor production rate C from *Merdith et al.* (2021); sea level SL from *van der Meer et al.* (2017), *Marcilly et al.* (2022) and *Young et al.* (2022). Bottom: Time series of continental area in the tropics (A_{tropics} from *Scotese* (2021), mean surface temperature (T) and precipitation rate (P_{cont}) from *Valdes et al.* (2021), and flux of material eroded (Φ) from *Salles et al.* (2023b). The supercontinent phase is shown in grey.

mantle heterogeneity can modulate this effect (*Greff-Lefftz and Besse*, 2014).

In Pandora, TPW peaks 50 Myr after breakup, linked to the merging of two subduction zones that accelerates the dispersal of a continental block at velocities higher

than 15 cm yr^{-1}. On Earth, the possible existence of a Jurassic TPW peak about 50 Myr after breakup is debated (*Fu et al.*, 2022; *Vaes and van Hinsbergen*, 2025). The rapid northward motion of the Greater Indian plate (*Jokat et al.*, 2021), splitting from Gondwana, is comparable with the fast dispersal observed in Pandora. Whether this was caused by subduction zone merging within the Tethys Ocean that would have triggered a short-lived TPW acceleration remains undemonstrated (*Vaes and van Hinsbergen*, 2025).

The Pandora experiment provides a unified framework to evaluate long-standing hypotheses on Earth's tectonic–environmental coupling. The alternation between climate cooling during assembly and warming before and during breakup supports the geodynamic forcing hypothesis of long-term climate change. Collectively, our results suggest that large-scale environmental fluctuations of Earth emerge naturally from mantle dynamics, linking deep Earth processes to planetary habitability.

5 Conclusions

This study presents the first fully integrated simulation of an Earth-like planet's evolution through a complete supercontinent lifetime, loosely coupling mantle convection, tectonics, climate dynamics, and surface processes. Although not a strict replica of Earth, this synthetic planet reveals the deep interconnections between the planetary interior and surface systems. The simulation highlights the dominant role of mantle-driven processes in modulating long-term environmental evolution. The aggregation of continents is an expression of a very large-scale flow, which drives assembly towards low latitudes through TPW and reduces heat transfer efficiency through seafloor aging. Combining these effects produces higher albedo, greater weatherability, and lower degassing. The aggregation state of the mantle is therefore expected to be concomitant with a cooler climate. Conversely, continents disperse through smaller-scale mantle flow, which drives higher heat transfer efficiency expected to produce larger degassing through an increase in seafloor production rates. This leads to higher sea level and hence a smaller weatherable area. The breakup state is therefore expected to correspond to a hotter climate.

These findings are consistent with geological and geochemical evidence from past supercontinents of the Earth, offering a robust mechanistic framework to interpret its deep-time evolution. They suggest that mantle dynamics can drive major environmental transitions, including alternations between greenhouse and icehouse states, without requiring external forcing. We suggest that the transition into the assembly state begins before the supercontinent stage, when mantle flow develops a hemispheric pattern. This state corresponds to mantle warming and atmospheric cooling. Conversely, the transition toward breakup starts before continents split, with the rejuvenation of the seafloor. This state corresponds to mantle cooling and atmospheric warming.

These major changes across the lifetime of supercontinents call for a revised understanding of the physical environment, and therefore of the abiotic controls for biological evolution and diversification (*Rogger et al.*, 2024; *Lorcery et al.*, 2025). Finally, the comparison between Pandora and Earth underscores the need for dynamically consistent deep-time reconstructions of seafloor spreading and paleo-elevation, paving the way for improved models of Earth's long-term climate stability and habitability. By bridging deep-Earth and surface processes, the framework integrating self-consistent geodynamic models with Earth system models opens new opportunities to probe the co-evolution of geodynamics, climate, and habitability on Earth and other rocky planets across geological timescales.

Acknowledgements

We thank Douwe van Hinsbergen and an anonymous reviewer for constructive reviews that helped us significantly improve the manuscript. N.C. received support from a European Research Council (ERC) advanced grant, award number 101142672. L.P. received support from the Center for the Origin and Prevalence of life (COPL) of ETH Zürich. S.Z. was supported by Australian Research Council grant DE210100084 and a University of Sydney Robinson Fellowship.

Author contributions

All authors contributed to the conceptualization, software, formal analysis and writing.

Data availability

The data that support the findings of this study are openly available at https://osf.io/j8dav.

Competing interests

The authors declare no conflicts of interest.

Copyright notice

© Author(s) 2026. This article is distributed under the Creative Commons Attribution 4.0 International License, which permits unrestricted use, distribution, and reproduction in any medium, provided the original author(s) and source are credited, and any changes made are indicated.

References

Arnould, M., N. Coltice, N. Flament, V. Seigneur, and R. D. Müller (2018), On the scales of dynamic topography in whole-mantle convection models, *Geochemistry, Geophysics, Geosystems: G(3)*, *19*(9), 3140–3163, doi: http://doi.org/10.1029/2018gc007516.

Arnould, M., N. Coltice, N. Flament, and C. Mallard (2020), Plate tectonics and mantle controls on plume dynamics, *Earth and Planetary Science Letters*, *547*(116439), 116,439, doi: http://doi.org/10.1016/j.epsl.2020.116439.

Arnscheidt, C. W., and D. H. Rothman (2022), Presence or absence of stabilizing Earth system feedbacks on different time scales, *Science Advances*, *8*(46), eadc9241, doi: http://doi.org/10.1126/sciadv.adc9241.

Balay, S., J. Brown, K. Buschelman, V. Eijkhout, W. Gropp, D. Kaushik, M. Knepley, L. McInnes, B. F. Smith, and H. Zhang (2012), *PETSc users manual*, Argonne National Laboratory.

Blakey, R. C. (2008), Gondwana paleogeography from assembly to

breakup—A 500 m.y. odyssey, in *Resolving the Late Paleozoic Ice Age in Time and Space*, pp. 1–28, Geological Society of America, doi: http://doi.org/10.1130/2008.2441(01).

Bradley, D. C. (2011), Secular trends in the geologic record and the supercontinent cycle, *Earth-Science Reviews*, *108*(1-2), 16–33, doi: http://doi.org/10.1016/j.earscirev.2011.05.003.

Bufe, A., J. K. C. Rugenstein, and N. Hovius (2024), CO2 drawdown from weathering is maximized at moderate erosion rates, *Science (New York, N.Y.)*, *383*(6687), 1075–1080, doi: http://doi.org/10.1126/science.adk0957.

Clift, P., and P. Vannucchi (2004), Controls on tectonic accretion versus erosion in subduction zones: Implications for the origin and recycling of the continental crust: SUBDUCTION TECTONICS, *Reviews of Geophysics (Washington, D.C.: 1985)*, *42*(2), doi: http://doi.org/10.1029/2003rg000127.

Coltice, N., B. R. Phillips, H. Bertrand, Y. Ricard, and P. Rey (2007), Global warming of the mantle at the origin of flood basalts over supercontinents, *Geology*, *35*(5), 391, doi: http://doi.org/10.1130/g23240a.1.

Coltice, N., L. Husson, C. Faccenna, and M. Arnould (2019), What drives tectonic plates?, *Science Advances*, *5*(10), eaax4295, doi: http://doi.org/10.1126/sciadv.aax4295.

Conrad, C. P. (2013), The solid Earth's influence on sea level, *Geological Society of America Bulletin*, *125*(7-8), 1027–1052, doi: http://doi.org/10.1130/b30764.1.

Conrad, C. P., and C. Lithgow-Bertelloni (2002), How mantle slabs drive plate tectonics, *Science (New York, N.Y.)*, *298*(5591), 207–209, doi: http://doi.org/10.1126/science.1074161.

Crowley, T. J. (1994), Pangean climates, in *Geological Society of America Special Papers*, Geological Society of America Special Papers, pp. 25–40, Geological Society of America, doi: http://doi.org/10.1130/spe288-p25.

Edwards, N. R., and R. Marsh (2005), Uncertainties due to transport-parameter sensitivity in an efficient 3-D ocean-climate model, *Climate Dynamics*, *24*(4), 415–433, doi: http://doi.org/10.1007/s00382-004-0508-8.

Evans, D. A. D. (2021), Meso-Neoproterozoic Rodinia supercycle, in *Ancient Supercontinents and the Paleogeography of Earth*, edited by L. J. Pesonen, J. Salminen, S.-A. Elming, D. A. D. Evans, and T. Veikkolainen, pp. 549–576, Elsevier, doi: http://doi.org/10.1016/b978-0-12-818533-9.00006-0.

Forsyth, D., and S. Uyeda (1975), On the relative importance of the driving forces of plate motion, *Geophysical Journal International*, *43*(1), 163–200, doi: http://doi.org/10.1111/j.1365-246x.1975.tb00631.x.

Fraedrich, K., E. Kirk, and F. Lunkeit (1998), Portable University Model of the Atmosphere (PUMA), *Tech. rep.*, Deutsches Klimarechenzentrum.

Fraedrich, K., H. Jansen, E. Kirk, U. Luksch, and F. Lunkeit (2005), The Planet Simulator: Towards a user friendly model, *Meteorologische Zeitschrift*, *14*(3), 299–304, doi: http://doi.org/10.1127/0941-2948/2005/0043.

Frasson, T., S. Labrosse, H.-C. Nataf, N. Coltice, and N. Flament (2024), On the impact of true polar wander on heat flux patterns at the core–mantle boundary, *Solid Earth*, *15*(5), 617–637, doi: http://doi.org/10.5194/se-15-617-2024.

Fu, H., S. Zhang, D. J. Condon, and H. Xian (2022), Secular change of true polar wander over the past billion years, *Science Advances*, *8*(41), eabo2753, doi: http://doi.org/10.1126/sciadv.abo2753.

Goddéris, Y., and Y. Donnadieu (2019), A sink- or a source-driven carbon cycle at the geological timescale? Relative importance of palaeogeography versus solid Earth degassing rate in the Phanerozoic climatic evolution, *Geological Magazine*, *156*(2), 355–365, doi: http://doi.org/10.1017/s0016756817001054.

Goddéris, Y., Y. Donnadieu, S. Carretier, M. Aretz, G. Dera, M. Macouin, and V. Regard (2017), Onset and ending of the late Palaeozoic ice age triggered by tectonically paced rock weathering, *Nature Geoscience*, *10*(5), 382–386, doi: http://doi.org/10.1038/ngeo2931.

Goldreich, P., and A. Toomre (1969), Some remarks on polar wandering, *Journal of Geophysical Research*, *74*(10), 2555–2567, doi: http://doi.org/10.1029/jb074i010p02555.

Golonka, J., and D. Ford (2000), Pangean (Late Carboniferous–Middle Jurassic) paleoenvironment and lithofacies, *Palaeogeography, Palaeoclimatology, Palaeoecology*, *161*(1-2), 1–34, doi: http://doi.org/10.1016/s0031-0182(00)00115-2.

Greff-Lefftz, M., and J. Besse (2014), Sensitivity experiments on True Polar Wander, *Geochemistry, Geophysics, Geosystems: G(3)*, *15*(12), 4599–4616, doi: http://doi.org/10.1002/2014gc005504.

Grigné, C., S. Labrosse, and P. J. Tackley (2005), Convective heat transfer as a function of wavelength: Implications for the cooling of the Earth, *Journal of Geophysical Research*, *110*(B3), doi: http://doi.org/10.1029/2004jb003376.

Guillaume, B., S. Pochat, J. Monteux, L. Husson, and G. Choblet (2016), Can eustatic charts go beyond first order? Insights from the Permian–Triassic, *Lithosphere*, *8*(5), 505–518, doi: http://doi.org/10.1130/l523.1.

Gurnis, M. (1988), Large-scale mantle convection and the aggregation and dispersal of supercontinents, *Nature*, *332*(6166), 695–699, doi: http://doi.org/10.1038/332695a0.

Holden, P. B., N. R. Edwards, K. Fraedrich, E. Kirk, F. Lunkeit, and X. Zhu (2016), PLASIM–GENIE v1.0: a new intermediate complexity AOGCM, *Geoscientific Model Development*, *9*(9), 3347–3361, doi: http://doi.org/10.5194/gmd-9-3347-2016.

Holden, P. B., N. R. Edwards, T. F. Rangel, E. B. Pereira, G. T. Tran, and R. D. Wilkinson (2019), PALEO-PGEM v1.0: a statistical emulator of Pliocene–Pleistocene climate, *Geoscientific Model Development*, *12*(12), 5137–5155, doi: http://doi.org/10.5194/gmd-12-5137-2019.

Janin, A., N. Coltice, N. Chamot-Rooke, and J. Tierny (2025), Geodynamics of a global plate reorganization from topological data analysis, *Nature Geoscience*, *18*(10), 1041–1047, doi: http://doi.org/10.1038/s41561-025-01772-7.

Jellinek, A. M., A. Lenardic, and R. T. Pierrehumbert (2020), Ice, fire, or fizzle: The climate footprint of Earth's supercontinental cycles, *Geochemistry, Geophysics, Geosystems: G(3)*, *21*(2), e2019GC008,464, doi: http://doi.org/10.1029/2019gc008464.

Jokat, W., T. Altenbernd, G. Eagles, and W. H. Geissler (2021), The early drift of the Indian plate, *Scientific Reports*, *11*(1), 10,796, doi: http://doi.org/10.1038/s41598-021-90172-z.

Lenardic, A., L. Moresi, A. M. Jellinek, C. J. O'Neill, C. M. Cooper, and C. T. Lee (2011), Continents, supercontinents, mantle thermal

mixing, and mantle thermal isolation: Theory, numerical simulations, and laboratory experiments: CONTINENTS AND MANTLE THERMAL MIXING, *Geochemistry, Geophysics, Geosystems: G(3)*, *12*(10), doi: http://doi.org/10.1029/2011gc003663.

Lenardic, A., A. M. Jellinek, B. Foley, C. O'Neill, and W. B. Moore (2016), Climate-tectonic coupling: Variations in the mean, variations about the mean, and variations in mode, *Journal of Geophysical Research. Planets*, *121*(10), 1831–1864, doi: http://doi.org/10.1002/2016je005089.

Leonard, J., S. Zahirovic, P. B. Holden, T. Salles, N. R. Edwards, and C. A. Mallard (2025), Polar wander leads to large differences in past climate reconstructions, *Communications Earth & Environment*, *6*(1), 508, doi: http://doi.org/10.1038/s43247-025-02485-w.

Lorcery, M., L. Husson, T. Salles, S. Lavergne, O. Hagen, and A. Skeels (2025), Deep time evolution of the Latitudinal Diversity Gradient: Insights from mechanistic models, *PloS One*, *20*(9), e0332,766, doi: http://doi.org/10.1371/journal.pone.0332766.

Maierová, P., K. Schulmann, O. Lexa, S. Guillot, P. Štípská, V. Janoušek, and O. Čadek (2016), European Variscan orogenic evolution as an analogue of Tibetan-Himalayan orogen: Insights from petrology and numerical modeling, *Tectonics*, *35*(7), 1760–1780, doi: http://doi.org/10.1002/2015tc004098.

Marcilly, C. M., T. H. Torsvik, and C. P. Conrad (2022), Global Phanerozoic sea levels from paleogeographic flooding maps, *Gondwana Research: International Geoscience Journal*, *110*, 128–142, doi: http://doi.org/10.1016/j.gr.2022.05.011.

Merdith, A. S., S. E. Williams, A. S. Collins, M. G. Tetley, J. A. Mulder, M. L. Blades, A. Young, S. E. Armistead, J. Cannon, S. Zahirovic, and R. D. Müller (2021), Extending full-plate tectonic models into deep time: Linking the Neoproterozoic and the Phanerozoic, *Earth-Science Reviews*, *214*(103477), 103,477, doi: http://doi.org/10.1016/j.earscirev.2020.103477.

Mills, B. J. W., C. R. Scotese, N. G. Walding, G. A. Shields, and T. M. Lenton (2017), Elevated CO2 degassing rates prevented the return of Snowball Earth during the Phanerozoic, *Nature Communications*, *8*(1), 1110, doi: http://doi.org/10.1038/s41467-017-01456-w.

Montañez, I. P., and C. J. Poulsen (2013), The late Paleozoic ice age: An evolving paradigm, *Annual Review of Earth and Planetary Sciences*, *41*(1), 629–656, doi: http://doi.org/10.1146/annurev.earth.031208.100118.

Murphy, B. P., J. P. L. Johnson, N. M. Gasparini, and L. S. Sklar (2016), Chemical weathering as a mechanism for the climatic control of bedrock river incision, *Nature*, *532*(7598), 223–227, doi: http://doi.org/10.1038/nature17449.

Müller, R. D., B. Mather, A. Dutkiewicz, T. Keller, A. Merdith, C. M. Gonzalez, W. Gorczyk, and S. Zahirovic (2022), Evolution of Earth's tectonic carbon conveyor belt, *Nature*, *605*(7911), 629–639, doi: http://doi.org/10.1038/s41586-022-04420-x.

Nance, R. D. (2022), The supercontinent cycle and Earth's long-term climate, *Annals of the New York Academy of Sciences*, *1515*(1), 33–49, doi: http://doi.org/10.1111/nyas.14849.

Nance, R. D., J. B. Murphy, and M. Santosh (2014), The supercontinent cycle: A retrospective essay, *Gondwana Research: International Geoscience Journal*, *25*(1), 4–29, doi: http://doi.org/10.1016/j.gr.2012.12.026.

Pesonen, L. J. J., J. Salminen, S.-A. Elming, D. Evans, and T. Veikkolainen (Eds.) (2021), *Ancient supercontinents and the paleogeography of earth*, Elsevier Science Publishing, Philadelphia, PA, doi: http://doi.org/10.1016/c2018-0-03855-4.

Phillips, B. R., and N. Coltice (2010), Temperature beneath continents as a function of continental cover and convective wavelength, *Journal of Geophysical Research*, *115*(B4), doi: http://doi.org/10.1029/2009jb006600.

Ricard, Y., and W. Bai (1991), Inferring the viscosity and the 3-D density structure of the mantle from geoid, topography and plate velocities, *Geophysical Journal International*, *105*(3), 561–571, doi: http://doi.org/10.1111/j.1365-246x.1991.tb00796.x.

Ricard, Y., G. Spada, and R. Sabadini (1993), Polar wandering of a dynamic earth, *Geophysical Journal International*, *113*(2), 284–298, doi: http://doi.org/10.1111/j.1365-246x.1993.tb00888.x.

Richardson, A., C. N. Hill, and J. T. Perron (2014), IDA: An implicit, parallelizable method for calculating drainage area, *Water Resources Research*, *50*(5), 4110–4130, doi: http://doi.org/10.1002/2013wr014326.

Rogger, J., E. J. Judd, B. J. W. Mills, Y. Goddéris, T. V. Gerya, and L. Pellissier (2024), Biogeographic climate sensitivity controls Earth system response to large igneous province carbon degassing, *Science (New York, N.Y.)*, *385*(6709), 661–666, doi: http://doi.org/10.1126/science.adn3450.

Rolf, T., N. Coltice, and P. J. Tackley (2012), Linking continental drift, plate tectonics and the thermal state of the Earth's mantle, *Earth and Planetary Science Letters*, *351-352*, 134–146, doi: http://doi.org/10.1016/j.epsl.2012.07.011.

Rolf, T., N. Coltice, and P. J. Tackley (2014), Statistical cyclicity of the supercontinent cycle, *Geophysical Research Letters*, *41*(7), 2351–2358, doi: http://doi.org/10.1002/2014gl059595.

Salles, T. (2019), ESCAPE: Regional to global scale landscape evolution model v2.0, *Geoscientific Model Development*, *12*(9), 4165–4184, doi: http://doi.org/10.5194/gmd-12-4165-2019.

Salles, T., X. Ding, and G. Brocard (2018), pyBadlands: A framework to simulate sediment transport, landscape dynamics and basin stratigraphic evolution through space and time, *PloS One*, *13*(4), e0195,557, doi: http://doi.org/10.1371/journal.pone.0195557.

Salles, T., C. Mallard, and S. Zahirovic (2020), gospl: Global Scalable Paleo Landscape Evolution, *Journal of Open Source Software*, *5*(56), 2804, doi: http://doi.org/10.21105/joss.02804.

Salles, T., L. Husson, P. Rey, C. Mallard, S. Zahirovic, B. H. Boggiani, N. Coltice, and M. Arnould (2023a), Hundred million years of landscape dynamics from catchment to global scale, *Science (New York, N.Y.)*, *379*(6635), 918–923, doi: http://doi.org/10.1126/science.add2541.

Salles, T., L. Husson, M. Lorcery, and B. Hadler Boggiani (2023b), Landscape dynamics and the Phanerozoic diversification of the biosphere, *Nature*, *624*(7990), 115–121, doi: http://doi.org/10.1038/s41586-023-06777-z.

Scotese, C. R. (2021), An atlas of Phanerozoic paleogeographic maps: The seas come in and the seas go out, *Annual Review of Earth and Planetary Sciences*, *49*(1), 679–728, doi: http://doi.org/10.1146/annurev-earth-081320-064052.

Scotese, C. R., H. Song, B. J. W. Mills, and D. G. van der

Meer (2021), Phanerozoic paleotemperatures: The earth's changing climate during the last 540 million years, *Earth-Science Reviews*, *215*(103503), 103,503, doi: http://doi.org/10.1016/j.earscirev.2021.103503.

Seton, M., S. E. Williams, M. Domeier, A. S. Collins, and K. Sigloch (2023), Deconstructing plate tectonic reconstructions, *Nature Reviews. Earth & Environment*, *4*(3), 185–204, doi: http://doi.org/10.1038/s43017-022-00384-8.

Sun, Y., M. M. Joachimski, P. B. Wignall, C. Yan, Y. Chen, H. Jiang, L. Wang, and X. Lai (2012), Lethally hot temperatures during the Early Triassic greenhouse, *Science (New York, N.Y.)*, *338*(6105), 366–370, doi: http://doi.org/10.1126/science.1224126.

Tackley, P. J. (2008), Modelling compressible mantle convection with large viscosity contrasts in a three-dimensional spherical shell using the yin-yang grid, *Physics of the Earth and Planetary Interiors*, *171*(1-4), 7–18, doi: http://doi.org/10.1016/j.pepi.2008.08.005.

Tetley, M. G., S. E. Williams, M. Gurnis, N. Flament, and R. D. Müller (2019), Constraining absolute plate motions since the Triassic, *Journal of Geophysical Research. Solid Earth*, *124*(7), 7231–7258, doi: http://doi.org/10.1029/2019jb017442.

Vaes, B., and D. J. J. van Hinsbergen (2025), Slow true polar wander around varying equatorial axes since 320 Ma, *AGU Advances*, *6*(2), e2024AV001,515, doi: http://doi.org/10.1029/2024av001515.

Valdes, P. J., C. R. Scotese, and D. J. Lunt (2021), Deep ocean temperatures through time, *Climate of the Past*, *17*(4), 1483–1506, doi: http://doi.org/10.5194/cp-17-1483-2021.

van Der Meer, D. G., R. E. Zeebe, D. J. J. van Hinsbergen, A. Sluijs, W. Spakman, and T. H. Torsvik (2014), Plate tectonic controls on atmospheric CO2 levels since the Triassic, *Proceedings of the National Academy of Sciences of the United States of America*, *111*(12), 4380–4385, doi: http://doi.org/10.1073/pnas.1315657111.

van der Meer, D. G., A. P. H. van den Berg van Saparoea, D. J. J. van Hinsbergen, R. M. B. van de Weg, Y. Godderis, G. Le Hir, and Y. Donnadieu (2017), Reconstructing first-order changes in sea level during the Phanerozoic and Neoproterozoic using strontium isotopes, *Gondwana Research: International Geoscience Journal*, *44*, 22–34, doi: http://doi.org/10.1016/j.gr.2016.11.002.

Veevers, J. J. (1990), Tectonic-climatic supercycle in the billion-year plate-tectonic eon: Permian Pangean icehouse alternates with Cretaceous dispersed-continents greenhouse, *Sedimentary Geology*, *68*(1-2), 1–16, doi: http://doi.org/10.1016/0037-0738(90)90116-b.

Wagenaar, S. D. M., B. Vaes, and D. J. J. van Hinsbergen (2025), Toward reconstructing mantle convection using a minimum-continent-motion reference frame, *Journal of Geophysical Research. Solid Earth*, *130*(12), e2024JB030,430, doi: http://doi.org/10.1029/2024jb030430.

Walker, J. C. G., P. B. Hays, and J. F. Kasting (1981), A negative feedback mechanism for the long-term stabilization of Earth's surface temperature, *Journal of Geophysical Research*, *86*(C10), 9776–9782, doi: http://doi.org/10.1029/jc086ic10p09776.

West, A. J. (2012), Thickness of the chemical weathering zone and implications for erosional and climatic drivers of weathering and for carbon-cycle feedbacks, *Geology*, *40*(9), 811–814, doi: http://doi.org/10.1130/g33041.1.

Williamson, M. S., T. M. Lenton, J. G. Shepherd, and N. R. Edwards (2006), An efficient numerical terrestrial scheme (ENTS) for Earth system modelling, *Ecological Modelling*, *198*(3-4), 362–374, doi: http://doi.org/10.1016/j.ecolmodel.2006.05.027.

Young, A., N. Flament, S. E. Williams, A. Merdith, X. Cao, and R. D. Müller (2022), Long-term Phanerozoic sea level change from solid Earth processes, *Earth and Planetary Science Letters*, *584*(117451), 117,451, doi: http://doi.org/10.1016/j.epsl.2022.117451.

Zhong, S., N. Zhang, Z.-X. Li, and J. H. Roberts (2007), Supercontinent cycles, true polar wander, and very long-wavelength mantle convection, *Earth and Planetary Science Letters*, *261*(3-4), 551–564, doi: http://doi.org/10.1016/j.epsl.2007.07.049.

Supplementary Materials

This section provides complementary material to the main text. Figure S1 shows the paleogeographic evolution of Pandora for the experiment with 1.5 Earth ocean volume and complements Figure 1 (1 Earth ocean volume). Figure S2 shows the apparent TPW path through the supercontinent cycle, and Figure S3 shows the locations of the 300 poles defining the random reference frames used for the statistical test in Figure 5. Figures S4 to S6 present the temperature, precipitation, and erosion/deposition fields for the three experiments not shown in the main text. Together with Figure 6, they cover all four combinations of ocean volume and reference frame. Figure S7 shows the time series of global surface evolutions for the 1.5 Earth ocean volume experiments, to be compared with Figure 4. Movies S1 to S10 showing surface evolutions of the models are available in the following repository: https://osf.io/j8dav.

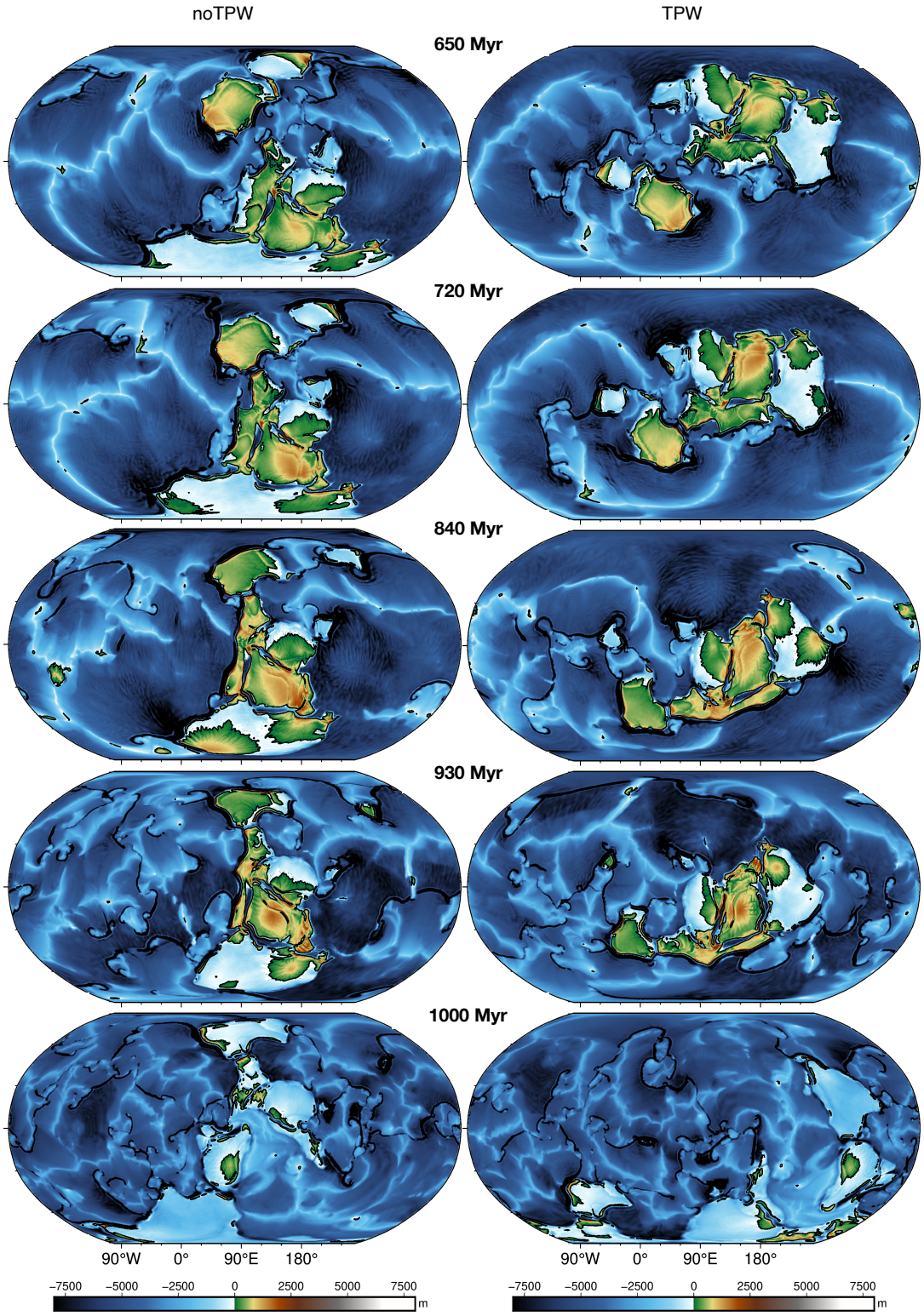


FIGURE S1 – Paleogeographic evolution of Pandora over supercontinent assembly and breakup using 1.5 Earth ocean volume.

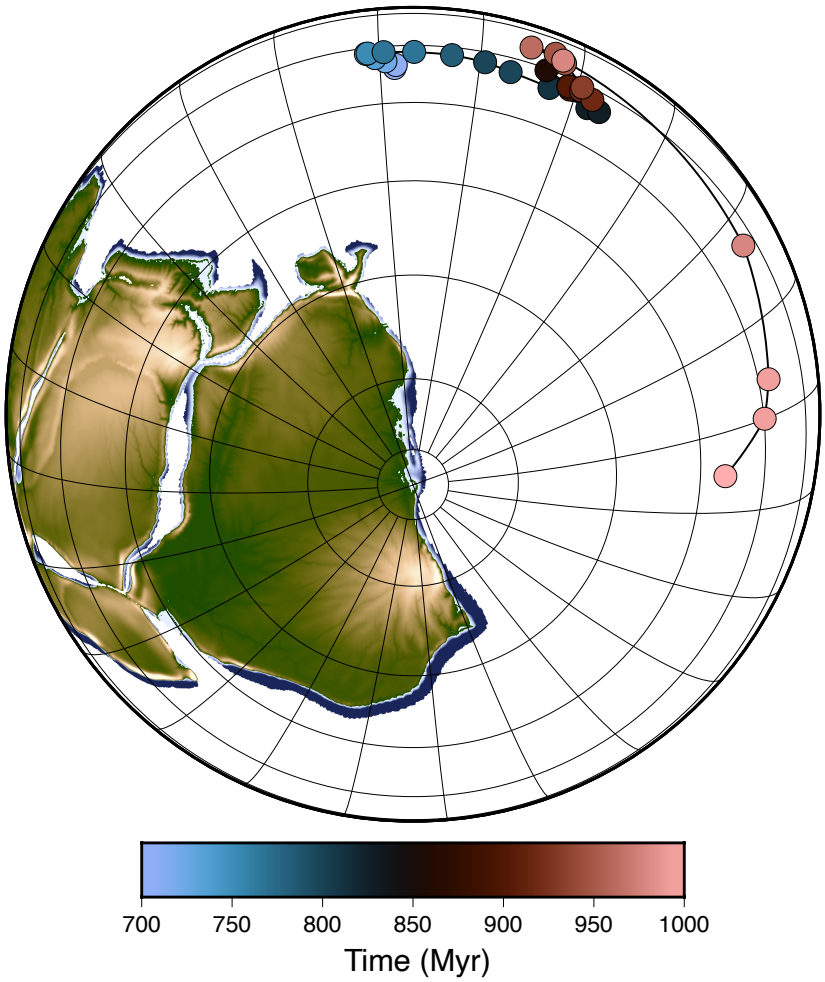


FIGURE S2 – Evolution of the apparent TPW path through the cycle, relative to the fixed supercontinent position at 720 Myr in Pandora.

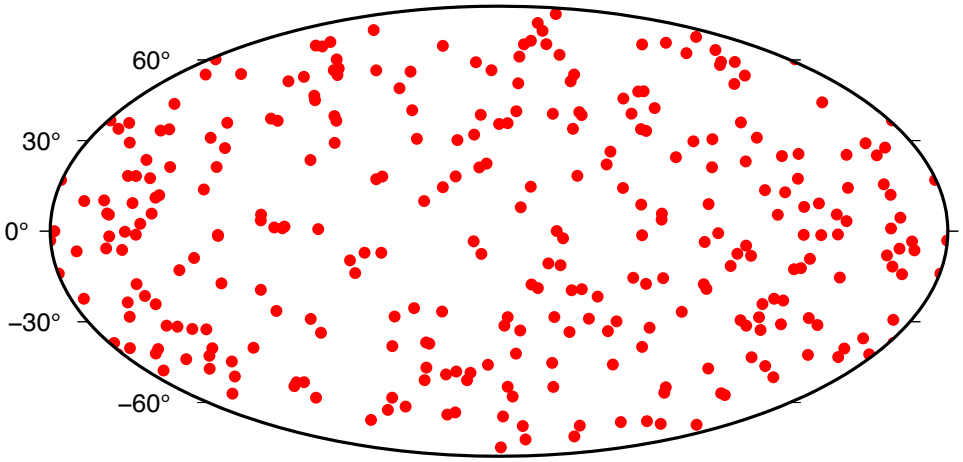


FIGURE S3 – Location of the 300 poles setting the random reference frames for the calculation of the geographical distribution of consumption rates.

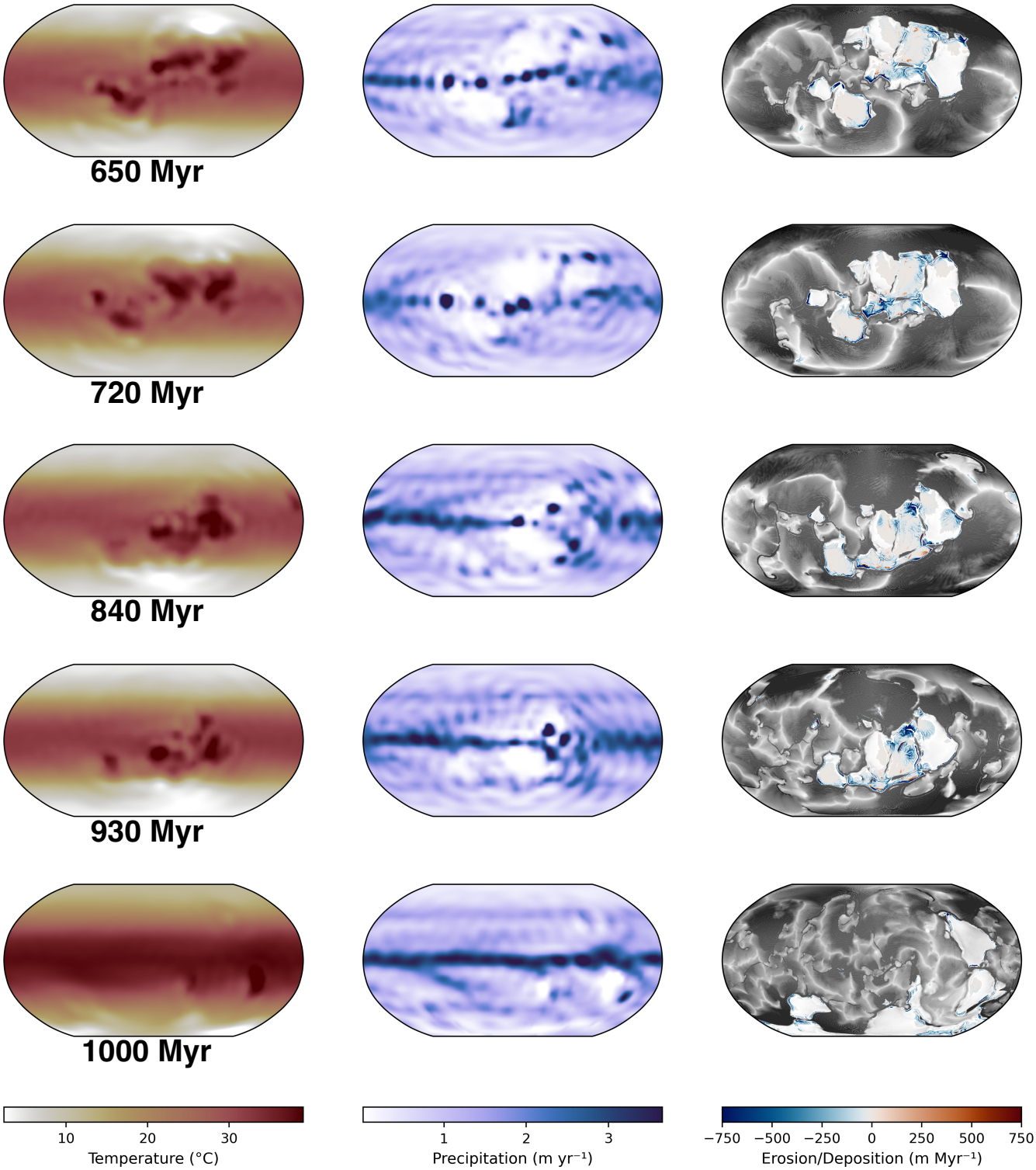


FIGURE S4 – Climate and surface processes evolution of Pandora over supercontinent assembly and breakup. The model is with 1.5 Earth ocean volume and accounts for TPW. Left column: Temperature. Central column: Precipitation. Right column: Erosion and deposition.

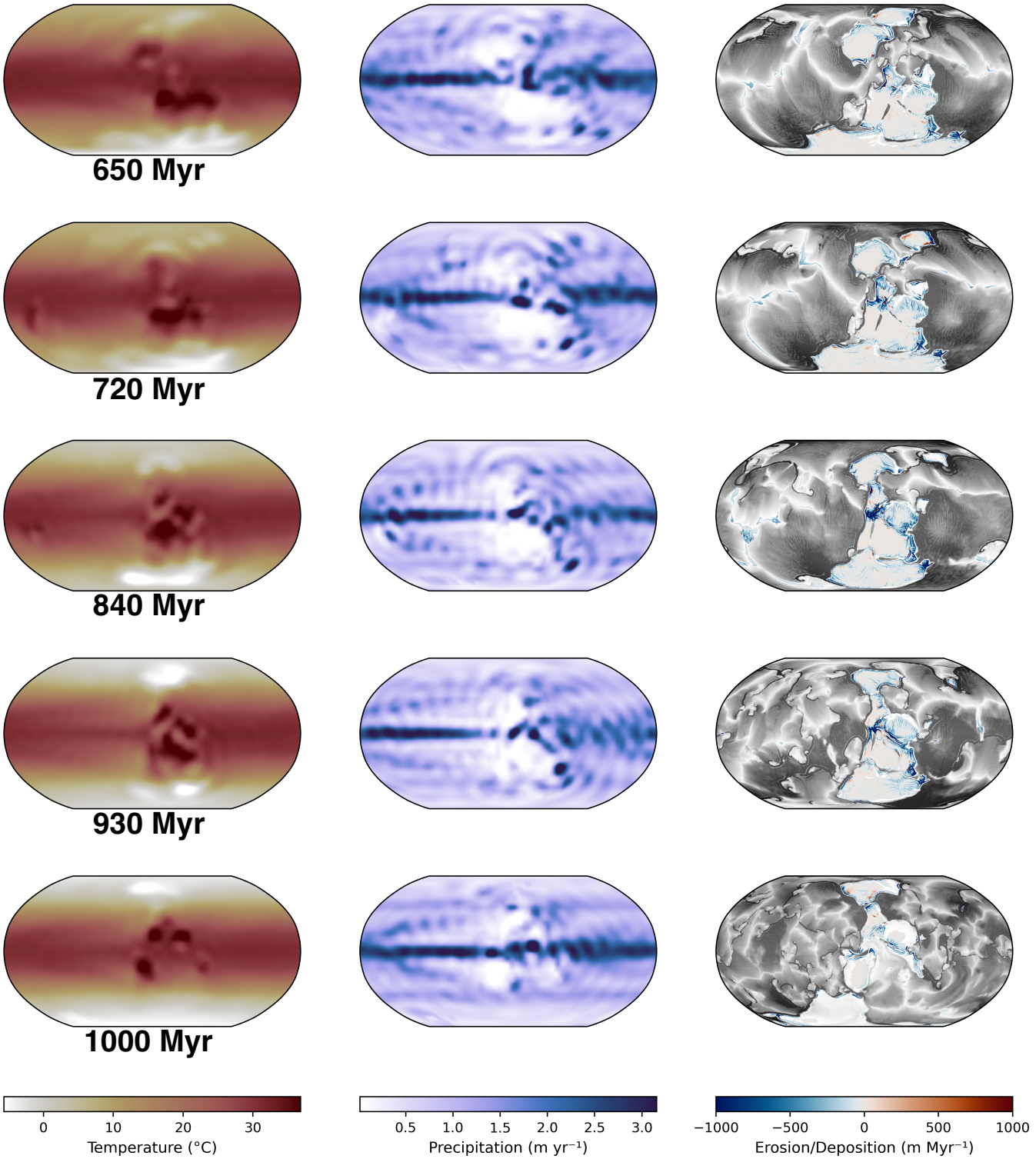


FIGURE S5 – Climate and surface processes evolution of Pandora over supercontinent assembly and breakup. The model is with 1 Earth ocean volume and without accounting for TPW. Left column: Temperature. Central column: Precipitation. Right column: Erosion and deposition.

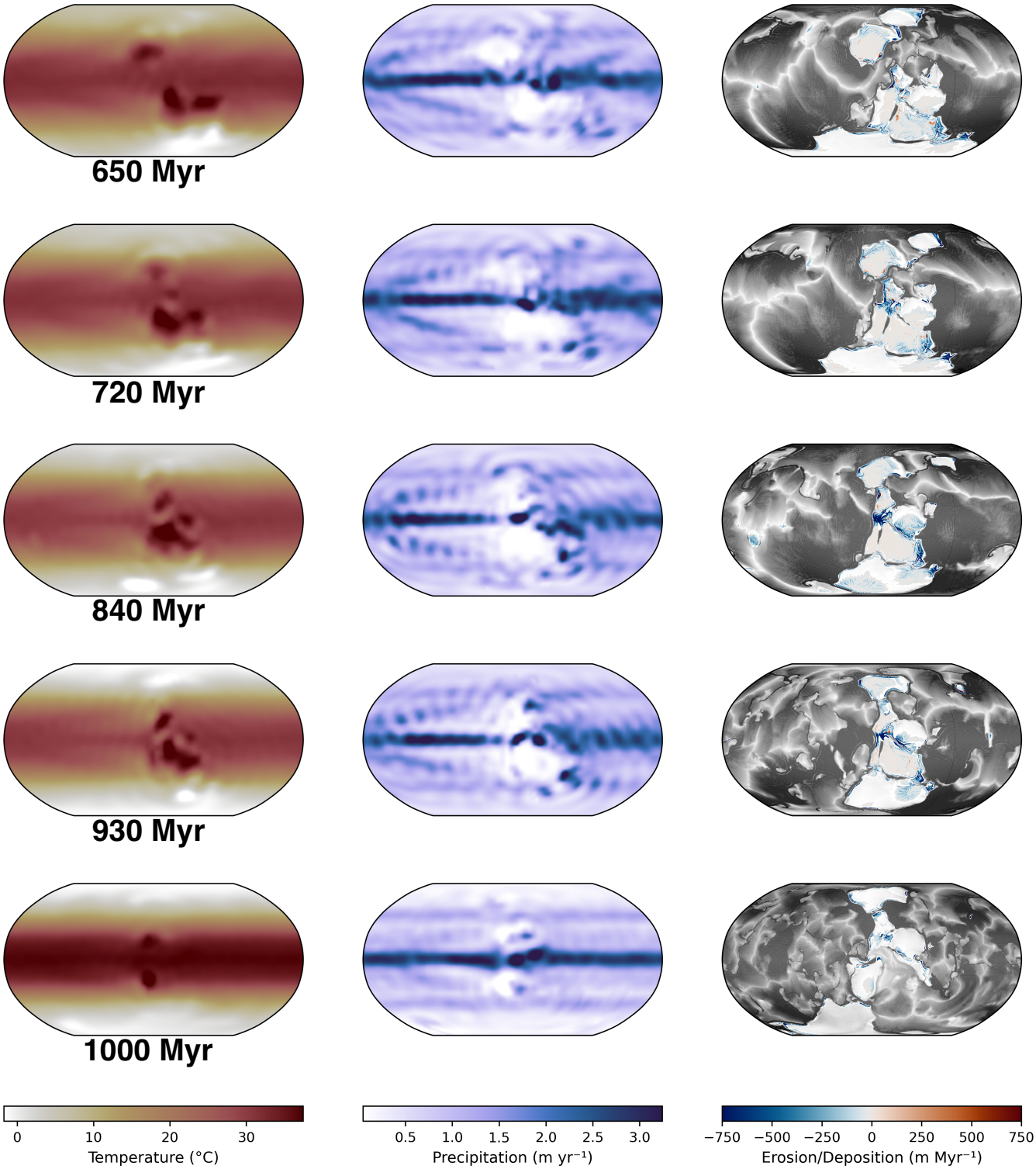


FIGURE S6 – Climate and surface processes evolution of Pandora over supercontinent assembly and breakup. The model is with 1.5 Earth ocean volume and without accounting for TPW. Left column: Temperature. Central column: Precipitation. Right column: Erosion and deposition.

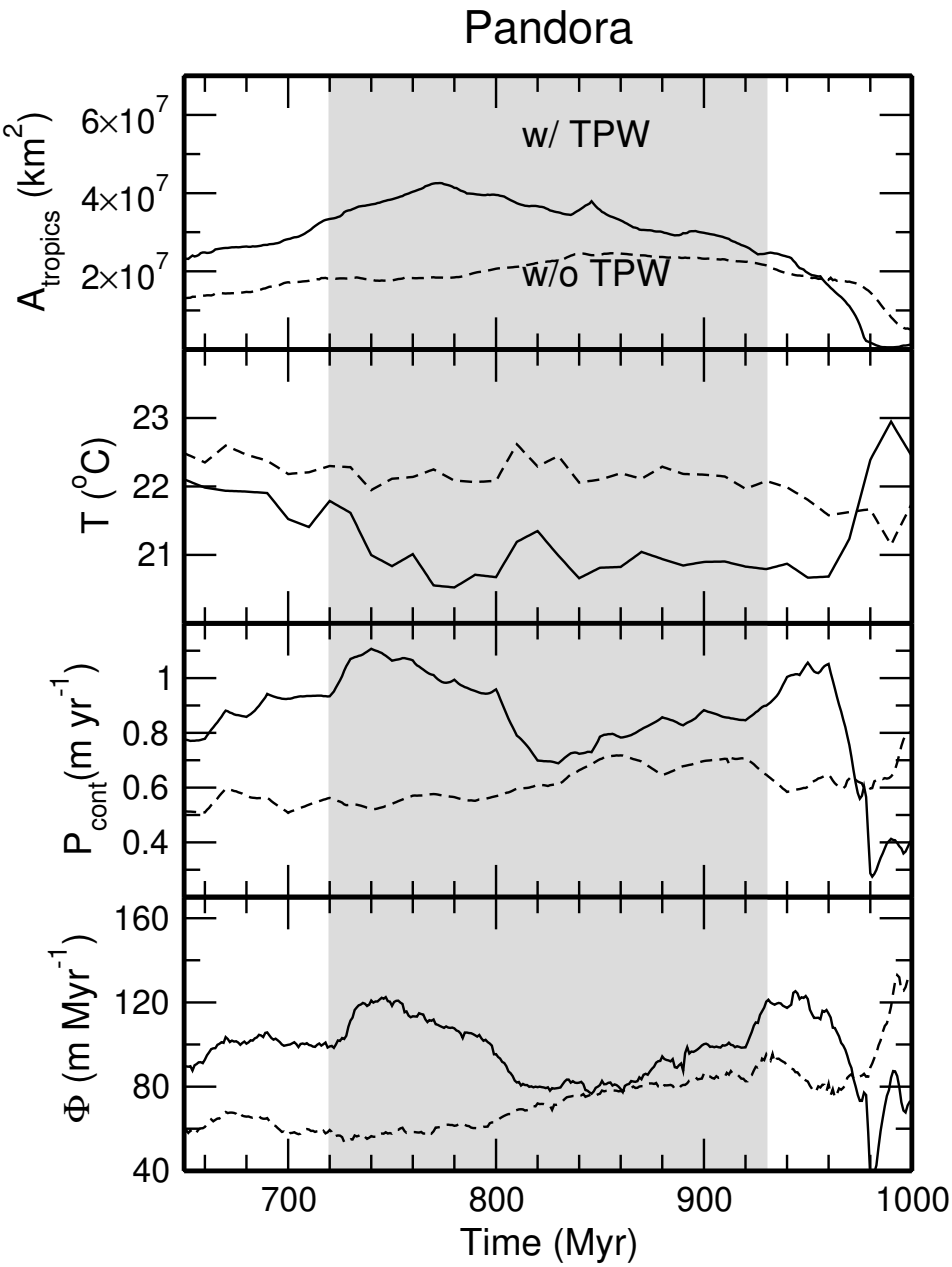


FIGURE S7 – Time series of continental area in the tropics ($A_{tropics}$), surface temperature (T), precipitations (P_{cont}), and flux of material eroded (ϕ) for Pandora (with and without accounting for TPW) using 1.5 Earth ocean volume. The supercontinent phases are shown by the grey shaded areas.

Supplementary Movies

Supplementary movies are in the following repository: https://osf.io/j8dav.

Caption for Movie S1: Evolution of elevation over the full modelled history following the spin-up phase of 250 Myr and until 1005 Myr. The study presented here then focuses on the supercontinent formation and dispersal being confined between 650 Myr and 1000 Myr.

Caption for Movie S2: Elevation evolution with TPW and 1 Earth ocean volume between 650 and 1000 Myr.

Caption for Movie S3: Elevation evolution without accounting for TPW and 1 Earth ocean volume between 650 and 1000 Myr.

Caption for Movie S4: Elevation evolution without accounting for TPW and 1.5 Earth ocean volume between 650 and 1000 Myr.

Caption for Movie S5: Surface temperature evolution with TPW and 1 Earth ocean volume between 650 and 1000 Myr.

Caption for Movie S6: Surface temperature evolution without accounting for TPW and 1 Earth ocean volume between 650 and 1000 Myr.

Caption for Movie S7: Precipitation evolution with TPW and 1 Earth ocean volume between 650 and 1000 Myr.

Caption for Movie S8: Precipitation evolution without accounting for TPW and 1 Earth ocean volume between 650 and 1000 Myr.

Caption for Movie S9: Erosion/deposition evolution with TPW and 1 Earth ocean volume between 650 and 1000 Myr.

Caption for Movie S10: Erosion/deposition evolution without accounting for TPW and 1 Earth ocean volume between 650 and 1000 Myr.